JOURNAL OF COLLOID AND INTERFACE SCIENCE **177,** 307–315 (1996)
ARTICLE NO. 0036

# Investigation of Mussel Adhesive Protein Adsorption on Polystyrene and Poly(octadecyl methacrylate) Using Angle Dependent XPS, ATR-FTIR, and AFM

ACE M. BATY,*,‡ PETER A. SUCI,* BONNIE J. TYLER,*,‡ AND GILL G. GEESEY*,†,[1]

**Center For Biofilm Engineering, 409 Cobleigh Hall, Montana State University, Bozeman, Montana 59717; †Department of Microbiology, 109 Lewis Hall, Montana State University, Bozeman, Montana, 59717; and ‡Department of Chemical Engineering, 306 Cobleigh Hall, Montana State University, Bozeman, Montana, 59717*

Received April 17, 1995; accepted June 28, 1995

**The irreversible adsorption of mussel adhesive proteins (MAP) from the marine mussel *Mytilus edulis* has been investigated on polystyrene (PS) and poly(octadecyl methacrylate) (POMA) surfaces using angle resolved X-ray photoelectron spectroscopy (XPS), attenuated total reflection Fourier transform infrared (ATR-FTIR) spectrometry, and atomic force microscopy (AFM). Angle resolved XPS was used to quantify the elemental composition with depth of the upper 90 Å of the surface, and AFM was used to obtain the surface topography. The adsorption pattern of MAP, revealed by AFM images, is distinctly different on the two polymer surfaces and suggests that the substratum influences protein adhesion. The depth profiles of MAP, obtained from angle resolved XPS, show differences in nitrogen composition with depth for MAP adsorbed to PS and POMA. Infrared spectra of hydrated adsorbed MAP revealed significant differences in the amide III region and in two bands which may originate from residues in the tandemly repeated sequences of MAP. This data demonstrates that the chemistry of the polymer film that is present at the protein–polymer interface can influence protein–protein and protein–surface interactions.** 

*Key Words:* **mussel adhesive protein; protein adsorption; XPS; ATR-FTIR; AFM.**

## INTRODUCTION

In the marine environment, microorganisms adhere tenaciously to virtually every known solid surface. Despite many years of research effort, the molecular interactions that are responsible for microbial adhesion and fouling of surfaces remain obscure. An understanding of these interactions would contribute to the development of surfaces that resist colonization of microorganisms. One reason why the molecular interactions are not understood is because microbial adhesion to surfaces is a multifactorial process that involves many types of bonding (1). To further complicate the situation, it has been shown that prior to microbial adhesion, a proteinaceous conditioning film forms on the surface of the substratum (2). This conditioning film imparts a uniform net negative charge to the surface and masks the substratum properties (3). The microorganisms attach to the conditioning film through adhesive structures composed of proteinaceous and exopolysaccharide molecules. Therefore, any serious study of microbial adhesion to submerged surfaces must include the characterization of molecular interactions with the conditioning film. Since the conditioning film which forms on the surface in the marine environment is still poorly defined, simplification of its composition is essential in order to provide for a degree of control that will enable the interactions at these surfaces to be characterized. The goal of this research is to characterize the interactions these proteins have when they are associated with two polymer surfaces displaying different functionalities, as is illustrated in Fig. 1.

The mussel adhesive proteins (MAP), which contain *Mytilus edulis* foot proteins one and two (MeFP-1 and MeFP-2), were used as a model protein conditioning film. MeFP-1 and MeFP-2 have a highly conserved repeat pattern. The MeFP-1 protein has a well-characterized structure consisting of repeating hexa- and decapeptide motifs and has an open conformation with very little secondary structure (4, 5). These qualities make this protein an ideal model conditioning film since the open conformation and repeat pattern makes the functional groups fully accessible for surface interactions. MeFP-1 and MeFP-2 also have novel compositions, with elevated levels of 3,4-dihydroxyphenyl-L-alanine (L-DOPA) and 4- and 3-mono- and di-transhydroxyproline (Hyp). These functional groups may confer an adhesive character to the proteins by enabling interactions using quinone redox chemistry (6, 7). However, these protein–surface interactions have yet to be demonstrated. Characterization of the specific protein–surface interactions is a prerequisite to the understanding of microbial attachment and fouling of surfaces.

## MATERIALS

### *Adsorbates, Solvents, and Substrates*

Purified MAP from *Mytilus edulis* was obtained from Swedish Bioscience Laboratory (Floda, Sweden) and stored

[1] To whom correspondence should be addressed.



0021-9797/96 $12.00

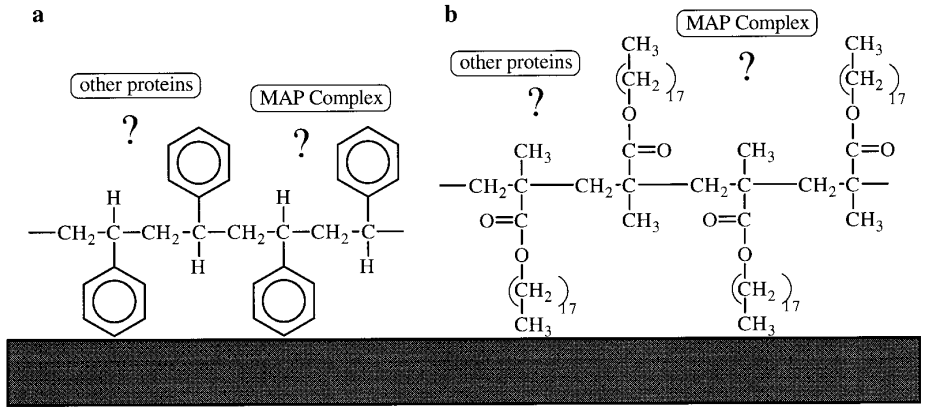


**FIG. 1.** Schematic diagram of the interactions being investigated between the MAP proteins (MeFP-1 and MeFP-2) and between the protein and polymer surfaces of (a) polystyrene and (b) poly(octadecyl methacrylate).

desiccated at −40°C. The amino acid composition according to the supplier is (per 1000 residues): 83 Asp, 74 Thr, 97 Ser, 64 Glu, 69 Pro, 132 Gly, 68 Ala, 50 Val, 25 Ile, 29 Leu, 30 Tyr, 12 Phe, 27 His, 115 Lys, 41 Arg, 41 Hyp, and 70 3,4-dihydroxy-L-phenylalanine (L-DOPA). Acetic acid-urea polyacrylamide gel electrophoresis (PAGE) indicated that the MAP preparation consisted of 80% of the two L-DOPA containing proteins, MeFP-1 and MeFP-2, in equal quantities. Two non-L-DOPA containing proteins contributed 20% of this preparation. The protocol for the PAGE was performed using previously described methods and the identification of MeFP-1 (130 kD) and MeFP-2 (45 kD) were made according to previously published results (8). Both MeFP-1 and MeFP-2 contain the unusual catecholic functionality L-DOPA.

Dichloromethylsilane (Aldrich 97%) was used as received. Hexadecane (Aldrich 99+%) was purified by passage through Super I Basic Alumina (Fisher Scientific) five times. All solvents including chloroform, ethanol, and toluene (Aldrich) were HPLC grade.

Optically smooth germanium (111) wafers (Exotic materials Inc., Costa Mesa, CA), 2.54 cm in diameter and 1-mm thick, were cut into 1 cm × 1 cm pieces using a diamond tipped stylus and spin coated with either polystyrene (PS) or poly(octadecyl methacrylate) (POMA) for the X-ray photoelectron spectroscopy (XPS) and atomic force microscopy (AFM) studies. For the attenuated total reflection Fourier transform infrared (ATR-FTIR) spectroscopy studies cylindrical germanium internal reflection elements (IRE) (Spectra Tech, Stamford, CT) were used.

PS (Aldrich Secondary Standard) was prepared as a 1.5% (w/v) solution in toluene. POMA (Aldrich) was prepared as a 1.5% (v/v) solution in toluene.

## PREPARATION OF SUBSTRATUM

### *Ge Cleaning Procedure*

The germanium crystals were immersed in an ultrasonic bath of a cleaning solution that was a mixture of isopropyl alcohol saturated with potassium hydroxide for 10 min. The crystals were then removed and immediately placed in an ultrasonic bath of ultra pure water. They were then gently scrubbed with undiluted Micro cleaning solution using cotton swabs. The crystals were rinsed in a hard stream of ultra pure water and immersed in a series of ultrasonic solvent baths, for 5 min each in ultra pure water (twice), ethanol, and chloroform. The crystals were then immediately dried under a stream of hydrocarbon free, dry nitrogen and transferred to an inert atmosphere (dry $N_2$) chamber, prior to silanization. The above cleaning procedure was performed immediately before the silanization reaction to prevent any adsorbed materials from contaminating the surface.

Auger electron spectroscopy, using a Phi Model 595 scanning Auger microprobe, indicated that the composition of the outermost surface region of the germanium substratum, when cleaned by this protocol, was 9.1 ± 1.4% carbon, 6.5 ± 2.0% oxygen, and 83.9 ± 2.2% germanium.

### *Silanization Procedure*

The germanium crystals were silanized with dichloromethylsilane to improve the adhesion of the polymer films and to prevent film delamination in aqueous solution. All silane monolayers were prepared under an inert atmosphere of dry $N_2$. Monolayers of dichloromethylsilane were formed by immersing clean Ge crystals into a freshly prepared solution of dichloromethylsilane in *n*-hexadecane. All glassware used was cleaned with ''piranha'' solution, consisting of a 70:30 mix of concentrated $H_2SO_4$ and 30% $H_2O_2$, respectively. [WARNING: Piranha solution reacts violently, even explosively with organic materials (9).] Individual solutions were prepared by mixing a solution that was $5 \times 10^{-3}$ *M* dichloromethylsilane in *n*-hexadecane. Each solution was stirred for 5 min before a germanium crystal was introduced. The reaction vessel was then capped and stored at room temperature for 12 h. Upon removal from the silane solution, the crystals were immediately rinsed with 50 ml of chloroform. They were then removed from the inert atmosphere

and extracted in a sohxlet extractor with hot chloroform for 30 min to remove any excess silane. They were then cured in an oven at 112°C for 3 h. Contact angle measurements were performed with water to estimate the quality of the silane film. Surfaces with contact angles less than 100° proved inadequate for polymer adhesion and were discarded.

*Preparation of Polymer Surfaces*

PS and POMA polymer films were spin cast onto presilanized, germanium fragments for the XPS and AFM studies. PS was used as a 1.5% (w/v) solution in toluene and POMA was used as a 1.5% (v/v) solution in toluene. Presilanized germanium crystals were completely covered with polymer solution and then immediately spin cast at 3500 rpm for 2 min. The polymer films were dried at room temperature for 24 h.

For the ATR-FTIR studies the cylindrical germanium IRE were silanized as described above. PS and POMA were dip coated onto germanium IRE at a speed of 0.5 cm/s.

X-ray photoelectron spectroscopy (Surface Science Instruments, Model SSX-100, 600-$\mu$m diameter spot size, monochromatized aluminum $K\alpha$ source) of the polymer films indicated that the films were continuous (i.e., no germanium or silane was detected). Recent AFM images acquired in the Fluid Tapping mode and cold-probe XPS analysis indicate that the spin cast polymer surfaces are stable when hydrated (manuscript in preparation).

*Protein Adsorption Protocol*

For the XPS and AFM studies the polymer coated germanium substrata were placed in a glass flow cell with entrance and exit tubing ports to allow for protein adsorption and subsequent rinse. For ATR-FTIR adsorption experiments, the polymer coated germanium IRE were placed within a stainless steel flow chamber (Circle Cell, Spectra Tech, Stamford, CT). Fluid was introduced and displaced through entrance and exit ports at each end of the Circle Cell.

All protein films were deposited onto freshly prepared polymer surfaces after the 24 h drying period. A stock solution of 1 mg/ml MAP was prepared in dilute HCl (pH 2.5) with deionized double distilled water, deaerated with $N_2$. The stock solution was stored at 5°C. A 50 $\mu$l aliquot of this solution was added to 0.45 ml of dilute HCl (pH 2.5). For the XPS and AFM studies this mixture was delivered into the flow cell containing the substratum that was to undergo protein adhesion. MAP was allowed to adsorb by raising the pH to 8.0 by delivering a 0.5 ml aliquot of a pH 10.9 solution into the reaction chamber, bringing the concentration of the protein to 50 $\mu$g/ml. For the ATR-FTIR studies a 50 $\mu$g/ml MAP solution was prepared as above before delivery into the flow cell. After a 1 h adsorption, the substratum was rinsed of any unadsorbed protein by flowing an aqueous solution at pH 8.0 through the reaction chamber at a rate of 100 ml/min for 3 min. The ATR-FTIR Circle Cell was rinsed at a rate of 0.5 ml/min for 60 min. The samples were removed and dried in hydrocarbon free dry air overnight.

## SURFACE CHARACTERIZATION

*Atomic Force Microscopy Imaging*

All surfaces were imaged using a Nanoscope III AFM (Digital Instruments, Inc., Santa Barbara, CA) with a 350D scanner and a 3-101 optical head. The instrument was used in contact mode using square pyramid microfabricated silicon nitride cantilevers which were 100 $\mu$m in length and had a spring constant of 0.38 N/m. The images were recorded using 1 $\mu$m $\times$ 1 $\mu$m and 5 $\mu$m $\times$ 5 $\mu$m scan areas at 512 scans per area with a scan rate of 2 $s^{-1}$. All images were acquired in air and were stable with time and reproducible.

*Angle Resolved X-Ray Photoelectron Spectroscopy*

XPS spectra were obtained from a Surface Science Instrument Model SSX-100 spectrometer. A 5 eV flood gun was used to offset charge accumulation on the samples. A 600-$\mu$m diameter spot size was scanned using a monochromatized Aluminum $K\alpha$ X-ray source at 350 W and pass energies between 25.0 eV (resolution 1) and 150 eV (resolution 4). Elemental composition was calculated on peak areas from the C 1*s*, N 1*s*, and O 1*s* core levels. Relative peak areas were calculated by fitting the high resolution C 1*s*, N 1*s*, and O 1*s* peaks with Gaussian functions. Before the variable angle study was conducted an initial survey at 80° (from the surface) was completed. Depth profiles were performed using variable angle XPS data collected at takeoff angles of 10°, 22°, 35°, and 80°. The elemental compositions at the initial 80° survey were compared with the final 80° angle study to ensure no X-ray damage had occurred during analysis. The data were collected with the wide angle acceptance lens masked with a 12° slit. The binding energy scale was referenced by setting the CHx peak maximum in the C 1*s* spectrum to 285.0 eV (10).

*ATR-FTIR Spectrometry*

The time course of MAP adsorption in a hydrated state was followed by ATR-FTIR spectrometry. During the time course of each experiment infrared (IR) spectra were acquired every 5 min. A Perkin Elmer Model 1800 Fourier transform infrared (FT-IR) spectrophotometer equipped with a liquid $N_2$ cooled, medium range mercury–cadmium–telluride detector (5000–580 $cm^{-1}$) was used to collect the ATR-FTIR spectra. Interferograms were double-sided, apodization was a weak Beer–Norton function, and the range was 4000–700 $cm^{-1}$ with an interval of 1 $cm^{-1}$ and nominal resolution of 2 $cm^{-1}$; 50 interferograms were averaged per spectrum. Water vapor bands were removed by subtraction of a pure water vapor spectrum; fluctuations in intensity of the strong water band at 1640 $cm^{-1}$ resulted in the appearance of this band in the difference spectra. This residual

water absorption band was removed by subtracting out a pure water spectrum using the ratio of areas of the absorption water band centered at 2120 $cm^{-1}$ as a normalization factor (11). Variation in absorbance values resulting from slight differences in alignment of the flow chamber on the optical bench and coating with polymer films were normalized by using the area of the water absorption band at 1640 $cm^{-1}$ (area: 1540 to 1740 $cm^{-1}$) as an internal standard (12). Areas of spectral features were computed for the region bounded by the data curve and a linear baseline drawn between the two endpoints of the integration.

Protein surface coverage was estimated based on area of the amide II band using published correlations. Adsorption conditions of Fink *et al.* (12) resemble approximately those here (saline solution, pH 7.4 on germanium). Extinction coefficients for solution phase bovine serum albumin compare favorably with our estimates (within 80%). Fink *et al.* (12) obtained correlations for adsorbed human albumin, immunoglobulin, and fibrinogen. Using their data, a factor for conversion of amide II areas to surface coverage in $\mu g/cm^2$ can be estimated. This conversion factor is $0.26 \pm 0.12$ $\mu g/cm^2$ per unit area amide II ($abs \cdot cm^{-1}$).

## RESULTS

### *Atomic Force Microscopy Imaging*

MAP adsorbed to clean PS and POMA from a solution with a bulk protein concentration of 50 $\mu$g/ml was imaged using AFM. Figure 2 shows AFM contour images of 1 $\mu$m $\times$ 1 $\mu$m areas of the two substrata before MAP adsorption (2a, 2d) and 1 $\mu$m $\times$ 1 $\mu$m (2b, 2e) and 5 $\mu$m $\times$ 5 $\mu$m (2c, 2f) areas after MAP adsorption. Before MAP adsorption, the polymer surfaces are extremely smooth with almost no surface features and with RMS surface roughness values of 1.035 and 0.546 nm for PS and POMA, respectively.

Adsorption of MAP to the PS surface resulted in the formation of closely packed, repeating structures as shown in Fig. 2b. Cross-sectional analysis of these features shows an average height of $9.48 \pm 3.05$ nm and a width of $33.02 \pm 7.82$ nm. The 5 $\mu$m $\times$ 5 $\mu$m scan area, shown in Fig. 2c, reveals that the features observed at high magnification cover larger areas of the surface, suggesting that the surfaces are homogeneous and have continuous protein coverage. In contrast, MAP adsorbed to the POMA surface displays very different protein features that appear to be linearly ordered as revealed in the 1 $\mu$m $\times$ 1 $\mu$m scan area in Fig. 2e. Cross-sectional analysis reveals that these features have an average height of $2.45 \pm 1.35$ nm and a width of $68.4 \pm 3.91$ nm. The 5 $\mu$m $\times$ 5 $\mu$m scan area, shown in Fig. 2f, shows the protein features on this surface to be very heterogeneous, with larger more complex fibrous structures. These features extend 19.36-nm high and 179.69 nm in width, with some as long as 2.4 $\mu$m. Because of the heterogeneous nature of MAP on this surface it is difficult to determine whether the surface coverage of the protein is continuous based on this technique.

### *Angle Resolved X-Ray Photoelectron Spectroscopy*

Angle dependent XPS of the surfaces studied in Fig. 2 further reveals the differences in MAP adsorption to PS and POMA surfaces. A detailed examination of the C 1*s* region of clean PS and POMA and of MAP adsorbed to PS and POMA at takeoff angles of 80° and 10° are given in Fig. 3. Each peak is contributed by different chemical groups. The C 1*s* peak at a binding energy of 291.6 eV is attributed to the pi–pi* transition in the aromatic rings of the polystyrene. The peak at 288.5 eV arises from the N—C═O and O—C═O functionalities on the protein and in the methacrylate chain, respectively. The C 1*s* peak at a biding energy of 286.6 eV is attributed to the C—N and C—O functionalities in the protein and the C—O—C functionality of the POMA. The dominant peak in both sets of spectra is at 285.0 eV. This peak originates from the aliphatic carbon in both the polymers and the protein.

Comparing the C 1*s* regions of MAP adsorbed to PS at 80° and 10° takeoff angles reveals a decrease in the aliphatic peak at 285.0 eV and disappearance of the peak associated with the pi–pi* transition. The disappearance of the pi–pi* transition and the decrease in the aliphatic peak relative to the 286.6 and 288.5 eV peaks from the protein indicates that at a takeoff angle of 10° the signal from the PS has disappeared from the spectra and signal intensity arises only from the protein. The C 1*s* region of MAP adsorbed to POMA reveals an increase in the peak at 286.6 eV relative to the 285.0 eV peak at the lower takeoff angle. This also indicates a greater contribution from the protein to this C 1*s* spectra.

The elemental compositions at the different angles were used with the calculated escape depths for each angle to gain insight on the elemental depth distribution of the proteins adsorbed to the polymer surfaces. The escape depths were calculated using parameters for organic compounds to calculate the inelastic mean free path and subsequently the escape depth using equations previously defined (13). Table 1 indicates that nitrogen is increasing with depth when MAP is adsorbed to PS, whereas, this trend is reversed on POMA. This indicates that MAP adsorbed to the polystyrene surface shows a nitrogen distribution that is enriched at the surface of the adsorbed protein film. In contrast, the MAP adsorbed to the POMA surface displays a depth profile that shows the nitrogen enrichment from the adsorbed protein at a maximum at the polymer surface.

### *ATR-FTIR Spectrometry*

Figures 4a and 4b show ATR-FTIR spectra of MAP adsorbed onto PS and POMA polymer films after the 60 min rinse period. The time course of adsorption/desorption was followed based on the areas (1591 to 1493 $cm^{-1}$) of the amide II band (indicated by (iii) in Figs. 4a and 4b). This

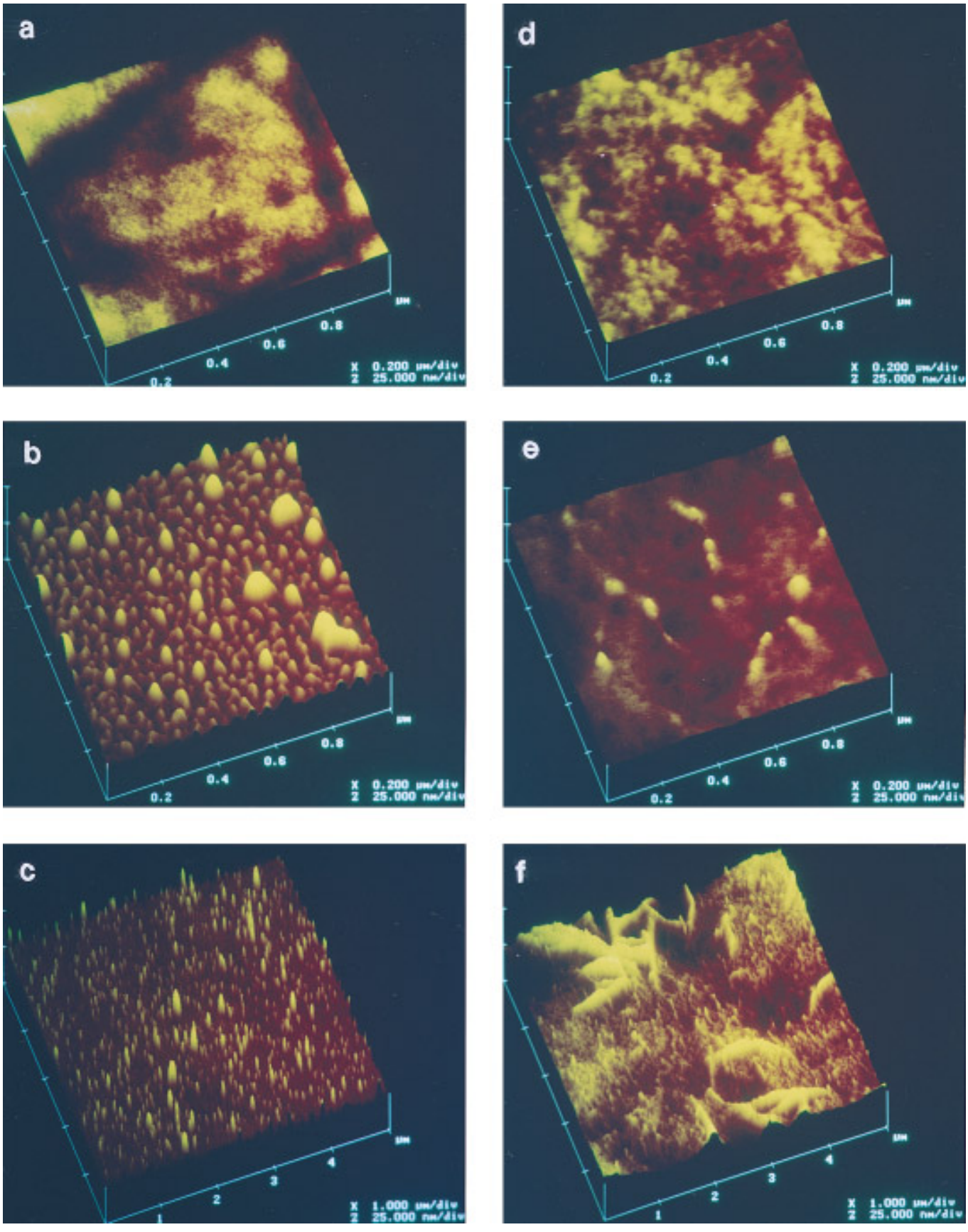


**FIG. 2.** AFM contour images of (a) 1 $\mu$m $\times$ 1 $\mu$m area of PS before protein adsorption, (b) 1 $\mu$m $\times$ 1 $\mu$m area of MAP adsorbed to PS, (c) 5 $\mu$m $\times$ 5 $\mu$m area of MAP adsorbed to PS, (d) 1 $\mu$m $\times$ 1 $\mu$m area of POMA before protein adsorption, (e) 1 $\mu$m $\times$ 1 $\mu$m area of MAP adsorbed to POMA, and (f) 5 $\mu$m $\times$ 5 $\mu$m area of MAP adsorbed to POMA.

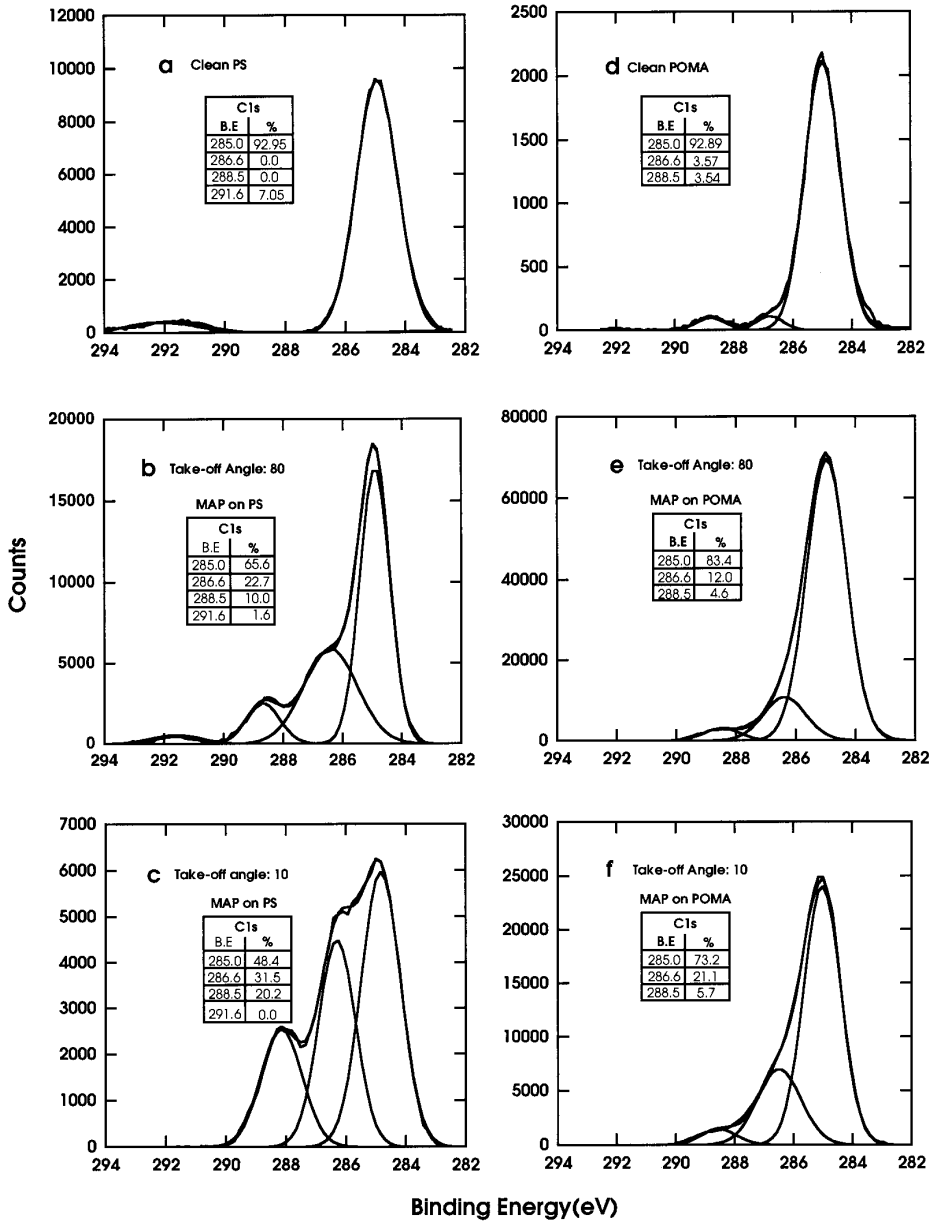


**FIG. 3.** C 1*s* spectra of clean PS (a) and POMA (d) and of MAP adsorbed to PS (b,c) and POMA (e, f ) at takeoff angles of 80° and 10°.

is shown in Fig. 4c for each of the two surfaces (PS and POMA). Adsorption appears to be irreversible. The surface coverage of MAP at the end of the rinse period on PS and POMA surfaces, estimated from the correlations specified in the Methods section, is $0.045 \pm 0.021$ and $0.066 \pm 0.031$ $\mu g/cm^2$, respectively.

Comparison of the spectra presented in Figs. 4a and 4b reveals a number of differences in spectral features. (Features are indicated in Figs. 4a and 4b by lower case Roman numerals.) A band centered at 1740 $cm^{-1}$ (i) is evident in MAP on POMA which does not appear in the spectrum of MAP on PS (although there is a slight band centered at 1730 $cm^{-1}$ in this spectrum). The amide I band (ii) is centered at 1645 and 1654 $cm^{-1}$ in the MAP on PS and POMA, respectively. Spectral features in the region from 1300 to 1200 $cm^{-1}$ (iv) are typically attributed to amide III vibrations which are sensitive to protein secondary structure (14–16) and less obscured by the large water band centered at 1640 $cm^{-1}$ than the amide I and II bands. In this region the spectrum of MAP on PS and POMA differ significantly. Distinct features centered at 1150 (v) and 1083 $cm^{-1}$ (vi) in both spectra are unusual for adsorbed proteins. The band centered at 1150 $cm^{-1}$ is especially prominent in the MAP on POMA.

## DISCUSSION

The results presented here, demonstrate that the functional groups that are present at a polymer surface can influence

**TABLE 1**

| Sample | Take-off angle | Escape depth | Mean atomic percent[a] C | O | N |
|---|---|---|---|---|---|
| MAP adsorbed to PS | 80 | 84.3 | 78.8 ± 6.3 | 13.5 ± 4.4 | 6.2 ± 3.2 |
| | 35 | 49.1 | 76.5 ± 7.5 | 15.8 ± 3.5 | 7.5 ± 3.6 |
| | 22 | 32.1 | 74.3 ± 8.4 | 16.0 ± 4.8 | 8.5 ± 4.3 |
| | 10 | 14.9 | 72.8 ± 8.5 | 16.7 ± 4.6 | 8.9 ± 4.2 |
| MAP adsorbed to POMA | 80 | 84.3 | 90.6 ± 1.5 | 6.2 ± 1.6 | 1.5 ± 0.1 |
| | 35 | 49.1 | 92.1 ± 0.6 | 6.6 ± 0.3 | 1.0 ± 0.1 |
| | 22 | 32.1 | 92.7 ± 0.4 | 6.5 ± 0.1 | 0.6 ± 0.1 |
| | 10 | 14.9 | 94.8 ± 0.6 | 4.7 ± 0.9 | 0.5 ± 0.5 |

[a] Taken from three separately prepared surfaces.

protein–protein and protein–surface interactions. The protein–surface interactions that can occur in the polymer–protein systems studied here are limited to two categories: one surface capable of undergoing MAP–surface pi–pi bond overlap interactions (PS) and one with no favorably energetic MAP–surface interactions (POMA). The PS surface provides a hydrophobic surface with an aromatic character and a medium surface free energy, and the POMA surface provides a hydrophobic low energy surface with an aliphatic functionality.

There are four mechanisms that have been proposed to play important roles in MAP–MAP and MAP–surface interactions: hydrogen bonding, metal-ligand complexes, Michael-type addition compounds derived from *o*-quinones, and charge transfer complexes (17). Olivieri *et al.* (18) have collected data that suggests that MAP can orient itself toward oxide surfaces enabling the L-DOPA residues to interact with the surface through hydrogen bonding. Hansen *et al.* (19) have recently found that MAP interacts with stainless steel by complexing and binding with surface metals. The Michael-type addition compounds are driven by the catechol oxidase enzyme that is cosecreted with the proteins in the natural system (20). In the system studied here, there are no divalent cations or metal ions to provide metal–ligand complexation. There are no enzyme driven reactions because the catechol oxidase does not survive the purification procedures for the MAP proteins and there are no functionalities present on the surface to allow hydrogen bonding interactions. However, at an elevated pH of 8 (approximately that of sea water and the pH during adsorption) the catechol functionality on the L-DOPA can undergo a spontaneous reverse dismutation to the *o*-quinone that is capable of interacting through a quinhydrone charge-transfer complex, illustrated in Fig. 5. The PS surface that displays an aromatic functionality would inhibit this MAP–MAP interaction because of the ability of PS to undergo pi–pi overlap interactions with the aromatic functionality of PS and the aromatic side chains of the MAP. The resulting surface topography after MAP adsorption to PS reveals homogeneous, repeating structures that would suggest this type of MAP–surface interaction. Furthermore, the dimensions of these features on the PS surface are representative of individual MeFP-1 and MeFP-2 molecules (21). In order to maximize the pi–pi interactions with the surface, the MAP will orient the aromatic side chains facing the polymer surface. This reasoning is supported by the decreasing nitrogen composition with depth in the XPS data. Since there are no energetically favorable MAP interactions with the POMA surface, the catecholic functional groups of the adsorbed protein are free to interact with each other and form charge-transfer complexes, as shown in Fig. 5. In this case the adsorption of the protein on a surface that appears to have no favorably energetic mechanisms for interactions is most likely driven by van der Waals forces, arising from the cross-linked protein with the surface. This results in the aggregated protein structures and the apparent linear order of the protein shown in the AFM images on this polymer surface. Furthermore, the smaller linear features on the POMA surface are representative of cross-linked MeFP-1 and MeFP-2 on the surface (21). The larger, fibrous structures on the POMA could arise from aggregated or cross-linked MAP. In either case, the AFM images suggest that the differences in surface chemistry on these two polymer surfaces strongly influence protein adsorption. Recent images obtained under fully hydrated conditions by AFM in Tapping Mode suggest that dehydration is not responsible for the gross differences observed by MAP on these surfaces.

When MAP adsorption to PS and POMA was evaluated under hydrating conditions by ATR-FTIR, spectral differences further suggested different protein interactions with the chemically distinct polymers. Differences in IR spectral features in the amide III region of proteins have been attributed to differences in secondary structure (14–16). Although it is difficult to make specific assignments unless the

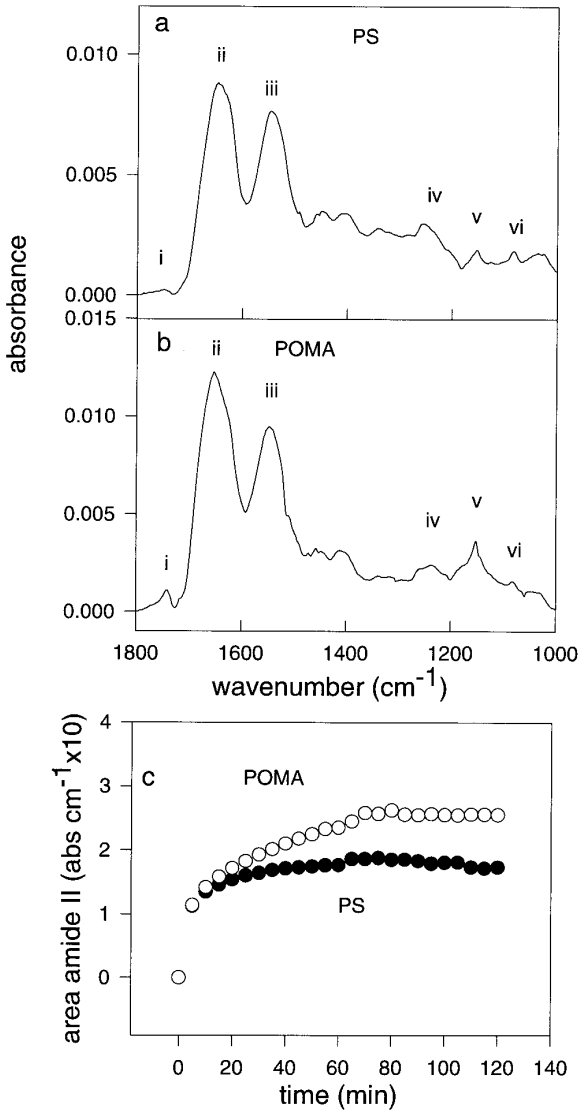


**FIG. 4.** ATR-FTIR spectra of adsorbed MAP to PS (a) and POMA (b). Roman numerals indicate spectral features discussed in the text. (c) Time course of adsorption (60 min) and rinse (60 min) followed by the area of the amide II band (iii). Open circles represent PS and closed circles POMA.

proteins consist entirely of one domain, differences observed in this amide III region (1200–1300 $cm^{-1}$) do indicate a difference in the hydrogen bonding pattern between the amide linkages of MAP on the PS and POMA surface. Therefore, the IR results are consistent with the XPS and AFM data which indicate that MAP organization and/or orientation are different on the PS and POMA surfaces. Of the three methodologies used, ATR-FTIR has the least spatial resolution. Since these spectral differences represent an average over the entire IRE surface (approx. 2.5 $cm^2$) it is unlikely that the phenomenon is confined to a small region of the surface.

The bands centered at 1150 and 1083 $cm^{-1}$ may originate from residues whose repetitive motif results in resonance summation at particular frequencies, making them visible above the background. An attempt to identify these bands as arising from specific residues by comparison with ATR-FTIR spectra of aqueous solutions of various compounds has so far been unsuccessful. Nevertheless, there is a resemblance between the contrasting spectral features which appear for MAP on PS and POMA and those reported for adsorption of the blood plasma protein, fibronectin, on a series of functionalized polyurethanes (15). Notably, differences were observed in the amide III and I regions, and a band appeared to varying degrees in the 1720–1740 $cm^{-1}$ region. The latter band arises from the carbonyl group and appears when a carboxylate functionality is protonated (i.e., salt to acid form) (22). For fibronectin, the appearance of this band was most prominent for the polyurethanes having the most hydrophobic functionalities. It was hypothesized that the acidic residues of the adsorbed protein entered a region of low dielectric constant proximal to the hydrophobic surface, shifting the equilibrium toward the protonated form. The MAP protein MeFP-2 is rich in acidic residues and it is speculated that it may mediate bridging between MeFP-1 (21). It is possible that the highly interconnecting pattern observed in the AFM images of MAP adsorbed to POMA results from this crosslinking reaction of MeFP-1 with MeFP-2.

Some degree of caution is necessary in interpreting the spectral features in the region from 1200 to 1300 $cm^{-1}$ as arising purely from the amide III resonance frequencies. Both L-DOPA and tyrosine exhibit bands in this region. In fact, the band at approximately 1250 $cm^{-1}$ has been previously attributed to the L-DOPA residues (18, 23). Therefore, the differences in this region for MAP on PS and POMA may indicate differences in the interaction between these residues and the polymer functional groups. These differences in protein–surface interactions between an aromatic surface (PS) and an aliphatic surface (POMA) are also indicated by the contrasting shape of the bands centered at 1150 and 1083 $cm^{-1}$.

The research presented here demonstrates that the functional groups that are present on the PS and POMA polymer surfaces will influence MAP–MAP and MAP–surface interactions. The XPS, AFM, and ATR-FTIR data demonstrates that differences in surface interactions can be correlated through these complementary analytical techniques.

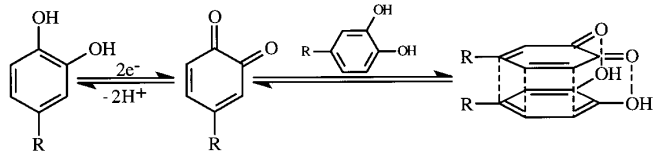


**FIG. 5.** Quinhydrone-charge transfer complex of the catechol functionality of MAP.

## ACKNOWLEDGMENTS

The authors gratefully acknowledge Joe A. Gardella Jr. and Pat Schamberger at SUNY Buffalo and Deborah Leach-Scampavia at NESA/BIO at the University of Washington for help with the XPS measurements. Also, thanks are extended to Kevin Siedlecki at MSU and Barney Drake and Clint Calahan at Imaging Services Inc. in Santa Barbara, CA for their help in AFM imaging. This work was sponsored by the Office of Naval Research under Grant N0014-93-1-0168, and the NSF under cooperative agreement EEC 8907039 and a grant to Gill G. Geesey from 3M.

## REFERENCES

1. McEldowney, S., and Fletcher, M., *Appl. Environ. Microbiol.* **52,** 460 (1986).
2. Baier, R. E., *in* ''Adsorption of Microorganisms to Surfaces'' (G. Bitton and K. C. Marshall, Eds.), p. 59. Wiley, New York, 1980.
3. Marshall, K. C., *ASM News* **58,** 202 (1992).
4. Waite, J. H., T. J. Housley, and M. L. Tanzer., *Biochemistry* **24,** 5010 (1985).
5. Taylor, S. W., Ross, M. M., Shabanowitz, J., Hunt, D. F., and Waite, J. H., *J. Am. Chem. Soc.* **116,** 10803 (1994).
6. Vogler, H., *Z. Naturfosch.* **386,** 1130 (1982).
7. Matsuda, H., Osaki, K., and Nitta, I., *Nippon Kogokukai Bull.* **31**(5), 611 (1958).
8. Waite, J. H., and C. V. Benedict, *Methods Enzymol.* **107,** 397 (1984).
9. Dobbs, D. A., Bergman, R. G., and Theopold, K. H., *Chem. Eng. News* **68**(17), 2 (1990).
10. Ratner, B. D., and Castner, D. G., *in* ''Surface Analysis-Techniques and Applications'' (J. C. Vickerman and N. M. Reed, Eds.), p. 163. Wiley, Chichester, UK, 1994.
11. Dousseau, F., Therien, M., and Pezolet, M., *Appl. Spectrosc.* **43,** 538 (1989).
12. Fink, D. J., Hutson, T. B., Chittur, K. K., and Gendreau, R. M., *Anal. Biochem.* **165,** 17 (1987).
13. Seah, M. P., Dench, W. A., Heydon and Son Ltd., *Surf. Interface Anal.* **2**(6) (1980).
14. Kaiden, K., Matsui, T., and Tanaka, S., *Appl. Spectrosc.* **41,** 180 (1987).
15. Jakobsen, R. J., and Wasacz, F. M., *in* ''Proteins at Interfaces: Physiochemical and Biochemical Studies'' (J. L. Brash and T. A. Horbett, Eds.), p. 339. Am. Chem. Soc., Washington, DC, 1987.
16. Pitt, W. G., Spiegelberg, S. H., and Cooper, S. L., *in* ''Proteins at Interfaces: Physiochemical and Biochemical Studies'' (J. L. Brash and T. A. Horbett, Eds.) p. 324. Am. Chem. Soc., Washington, DC, 1987.
17. Waite, J. H., *Int. J. Adhes. Adhes.* **7,** 9 (1987).
18. Olivieri, M. P., Loomis, R. E., and Baier, R. E., *Biomaterials* **13,** 1000 (1992).
19. Hansen, D. C., Luther III, G. W., and Waite, J. H., *J. Colloid Interface Sci.* **168,** 206 (1994).
20. Waite, J. H., *Int. J. Biol. Macromol.* **12,** 139 (1989).
21. Rzepecki, L. M., Hansen, K. M., and Waite, J. H., *Biol. Bull.* **183,** 123 (1992).
22. Parker, F. S. (Ed.), *in* ''Applications of Infrared, Raman, Resonance Raman in Biochemistry. Chapter 8, Carbohydrates'' p. 315. Plenum, New York, 1983.
23. Olivieri, M. P., Loomis, R. E., Meyer, A. E., and Baier, R. E., *J. Adhes. Sci. Technol.* **4,** 197 (1990).